Projected Increases in Summertime Temperature Variance are Driven by Local Thermodynamics

Lucas Vargas Zeppetello[1] and David S. Battisti[1]

[1]University of Washington

November 24, 2022

Abstract

The increasing frequency of very high temperatures driven by global warming has motivated growing interest in how the probability distribution of summertime temperatures will evolve in the future. Climate models predict increasing temperature variance in global warming simulations, but given their biased representations of historical temperature variability, it is important to use simple models to evaluate and understand these predictions. In this study we show that the projections of increasing temperature variance are indeed credible and are driven primarily by the magnitude of local warming. A simple analytic theory based on the surface energy and water budgets reproduces the increased midlatitude summertime temperature variance shown by state of the art climate models using only the local change in summertime mean temperature and relative humidity. The relative contributions of local warming and relative humidity changes to the increases in summertime temperature variance are roughly equal.

Projected Increases in Summertime Temperature Variance are Driven by Local Thermodynamics

L.R. Vargas Zeppetello[1], **D.S. Battisti**[1]

[1]Department of Atmospheric Sciences, University of Washington

Key Points:

- Summertime temperature variance over land increases with local mean temperature in contemporary global climate models.
- A theoretical model captures these increases using only projected changes in temperature and relative humidity from global climate models.
- Uncertainties in plant processes and climate sensitivity control the spread of climate model summertime temperature variance change.

Corresponding author: L.R. Vargas Zeppetello, `lvz7@uw.edu`

Abstract

The increasing frequency of very high temperatures driven by global warming has motivated growing interest in how the probability distribution of summertime temperatures will evolve in the future. Climate models predict increasing temperature variance in global warming simulations, but given their biased representations of historical temperature variability, it is important to use simple models to evaluate and understand these predictions. In this study we show that the projections of increasing temperature variance are indeed credible and are driven primarily by the magnitude of local warming. A simple analytic theory based on the surface energy and water budgets reproduces the increased midlatitude summertime temperature variance shown by state of the art climate models using only the local change in summertime mean temperature and relative humidity. The relative contributions of local warming and relative humidity changes to the increases in summertime temperature variance are roughly equal.

Plain Language Summary

Extreme summertime temperatures are a focal point for the impacts of climate change. Climate models project increasing summertime temperature variance in simulations driven by anthropogenic CO_2 forcing. If credible, these increases imply that extreme summertime temperatures will become even more frequent than a simple shift in the contemporary probability distribution would suggest. Given the impacts of extreme temperatures on public health, food security, and the global economy, it is of great interest to understand whether the projections of increased temperature variance are credible. In this study, we find that the large increases in summertime temperature variance projected by climate models are credible, predictable from first principles, and driven by local changes in summertime mean temperature and relative humidity.

1 Introduction

How will summertime land surface temperature variability evolve as the climate changes? This question is of paramount importance, not only for a more complete understanding land-atmosphere interaction, but for a more nuanced projection of how the frequency of heat waves and droughts will change in the future. Complicating our understanding of temperature variability over land is the fact that contemporary climate models show significant biases in their representations of summertime temperature variability. The ratio of the multi-model-mean (MMM) summertime temperature variance in 41 global climate models participating in the Coupled Model Intercomparrison Project Phase 6 (CMIP6, Eyring et al., 2016) to the variance observed over the last 20 years of the historical period (1995-2014) is shown in Fig. 1. The supplementary information contains a list of all models in the ensemble (Table S1). The models over-predict the summertime temperature variance by at least 20% over a considerable fraction of the midlatitudes; a similar value was found in an analysis of the CMIP5 ensemble (Vargas Zeppetello, Tétreault-Pinard, et al., 2020).

Debate over the dominant controls on summertime temperature variability is prevalent throughout the climate modelling literature. Studies of atmospheric dynamics have argued that thermal advection and steep gradients in land-ocean temperatures are responsible for shaping the distributions of above-boundary layer temperatures (Schneider et al., 2015; Linz et al., 2020). However, Holmes et al. (2016) found that thermal advection can explain only a small fraction of the increases in summertime temperature variance projected in CMIP5 models in global warming simulations. As atmospheric dynamics provides relatively little insight on how the contemporary pattern of summertime temperature variance will evolve in a changing climate, local processes related to surface soil moisture have been shown to contribute a significant amount of variability in climate models (e.g., Koster et al., 2006; Berg et al., 2014; Vogel et al., 2017). Donat et al. (2017)

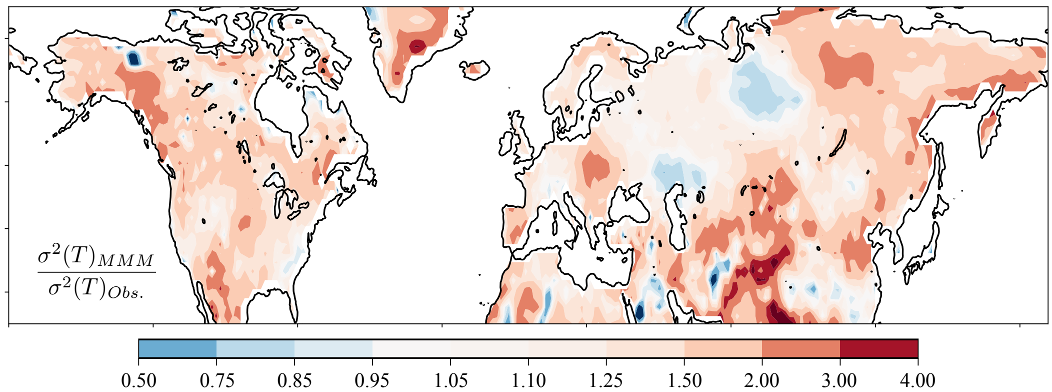

Figure 1. Summertime temperature variance bias defined as the ratio of the multi-model-mean variance from 41 CMIP6 models from 1994-2014 of historical simulations to observed temperature variance from gridded weather station observations from the same period (Willmott & Matsuura, 2001).

documented the connection between surface fluxes, soil moisture, and temperature variability in the CMIP5 ensemble, but also pointed out that changes in extreme temperatures represented in the models driven by the anthropogenic emissions during the historical period have not been observed; a problem that is likely linked to the biases in temperature variance documented Fig. 1. The biases in contemporary models and the consensus that soil moisture and surface fluxes are of paramount importance to temperature variability over land justify using simple models to understand the evolution of summertime temperature variance in a warming world.

In recent work, Vargas Zeppetello, Battisti, and Baker (2020) used the local surface energy and water budgets to derive a simple equation for summertime temperature variance as a function of monthly variability in shortwave radiation $\mathcal{F}$ and precipitation $\mathcal{P}$:

$$\sigma^2(T') = \frac{1}{\Gamma^2}\left[\sigma^2(\mathcal{F}') - 2\zeta\overline{\mathcal{F}'L\mathcal{P}'} + \zeta^2\sigma^2(L\mathcal{P}')\right] \ . \tag{1}$$

In Eq. 1, primed quantities represent deviations from monthly mean values in June, July, and August while σ^2 terms represent the variance, or average of the squares of these primed anomaly terms. Barred terms indicate summertime mean averages. The shortwave variance, precipitation variance and covariance between monthly anomalies in these two terms will be referred to as "forcing components" and are illustrated in the supplementary information (Fig. S1). Importantly, terms $\mathcal{F}'$ and $\mathcal{P}'$ are not independent, they are anti-correlated and the term $\overline{\mathcal{F}'L\mathcal{P}'}$ is negative and acts to increase the overall temperature variance. Γ [W m^{-2} K^{-1}] is a damping parameter that scales linearly with mean soil moisture, reflecting the fact that climatologically wet regions use more incident energy for evapotranspiration, thereby reducing surface temperature fluctuations (Seneviratne et al., 2010, and references therein). ζ (unitless) is a dryness index between zero and one that amplifies temperature variance associated with precipitation in dry regions. Precipitation-induced soil moisture anomalies preferentially amplify temperature variability in dry regions due to a combination of evapotranspiration's sensitivity to soil moisture in regions with low soil moisture and high atmospheric demand for water vapor (Seneviratne et al., 2010; Vargas Zeppetello et al., 2019). A brief derivation of this equation is found in the Appendix, and evaluation of the equation's capacity to replicate summertime temperature variance in the CMIP6 ensemble is provided in the supplementary information (Fig. S2).

Temperature Variance Sensitivity

In this section, we perform a sensitivity analysis of Eq. 1 to provide insight into how temperature variance will evolve as the climate warms. The partial derivative of Eq. 1 with respect to mean summertime temperature $\overline{T}$ is:

$$\frac{\partial \sigma^2(T')}{\partial \overline{T}} = \frac{2}{\Gamma^2}\left[\zeta \frac{\partial \zeta}{\partial \overline{T}} \sigma^2(L\mathcal{P}') - \overline{\mathcal{F}' L\mathcal{P}'}\frac{\partial \zeta}{\partial \overline{T}} - \Gamma \frac{\partial \Gamma}{\partial \overline{T}} \sigma^2(T')\right] . \tag{2}$$

This partial differentiation ignores potential contributions to changing temperature variance from the forcing components, summertime mean soil moisture, and model parameters. Thus, Eq. 2 represents *only* the change in temperature variance associated with climatological warming. Changes in the forcings parameters $\sigma^2(\mathcal{F})$ and $\sigma^2(\mathcal{P})$ are shown in the supplementary information (Fig. S3), but those changes could also be induced by local warming impacting boundary layer clouds over land (Laguë et al., 2019) and thus may not constitute a completely independent forcing on the land surface. Eq. 2 ignores changes in soil moisture; some authors attribute more extreme temperature variability in climate change simulations to large scale land surface drying (Vogel et al., 2017), but Berg et al. (2016) have shown that soil moisture changes in models are largely seasonal, reflecting an increased amplitude of the cycle of climatological precipitation minus evapotranspiration. Thus, soil moisture changes may also not constitute a purely independent forcing on the land surface in the same way as the climatological warming. The partial derivative in Eq. 2 provides a thermodynamic estimate based on purely local changes associated with atmospheric water vapor demand realized through the two parameters ζ and Γ:

$$\frac{\partial \zeta}{\partial \overline{T}} = \frac{\alpha}{(\overline{V}+\alpha)^2}\left(\frac{d\overline{q_s}}{d\overline{T}}(1-\overline{\mathrm{RH}}) - \overline{q_s}\frac{\partial \overline{\mathrm{RH}}}{\partial \overline{T}}\right) , \tag{3}$$

$$\frac{\partial \Gamma}{\partial \overline{T}} = \frac{L\rho_a \overline{m}}{r_s}\left(\frac{d^2\overline{q_s}}{d\overline{T}^2}(1-\zeta) - \frac{d\overline{q_s}}{d\overline{T}}\frac{\partial \zeta}{\partial \overline{T}}\right) . \tag{4}$$

In Eq. 3, α is a constant composed of various parameters that we assume are spatially invariant across the land surface (see Eq. A7), $\overline{m}$ is the mean soil moisture, and $\overline{V}$ is the summertime mean atmospheric water vapor demand calculated as $\overline{V} = q_s(\overline{T})(1-\overline{\mathrm{RH}})$ where $\overline{T}$ and $\overline{\mathrm{RH}}$ are the surface temperature and relative humidity, respectively.

The differentials in Eqs. 3 and 4 reflect different impacts of mean temperature change on local thermodynamics that impact the energetics of evapotranspiration. The change in ζ with mean temperature reflects the tendency towards a more arid climate both through increasing summertime mean saturation specific humidity $\overline{q_s}$ directly through the Clausius-Clapeyron's temperature dependence *and* modulating the climatological relative humidity $\overline{\mathrm{RH}}$. The change in Γ expresses the change in the land surface's capacity to mute forced energy perturbations due to changes in the climatological mean evapotranspiration.

Impact of Climate Change on Temperature Variance

To calculate the change in temperature variance expected purely from local warming, we calculate the derivatives in Eqs. 3 and 4 using CMIP6 MMM climatological $\overline{V}$, $\overline{m}$, $\overline{q_s}$, and $\overline{\mathrm{RH}}$ from the end of the historical period (1995-2014). We approximate $\frac{\partial \overline{\mathrm{RH}}}{\partial \overline{T}}$ by dividing the local MMM relative humidity change at the end of the 21st century by the local MMM warming $\Delta\overline{T}$. After calculating these derivatives, we substitute them into Eq. 2 and compute the total change in temperature variance as:

$$\Delta\sigma^2(T') = \frac{\partial \sigma^2(T')}{\partial \overline{T}}\Delta\overline{T} . \tag{5}$$

Figure 2a shows the CMIP6 multi-model-mean change in temperature variance between 2080-2099 of the SSP585 scenario and 1995-2014 of the historical simulations, while

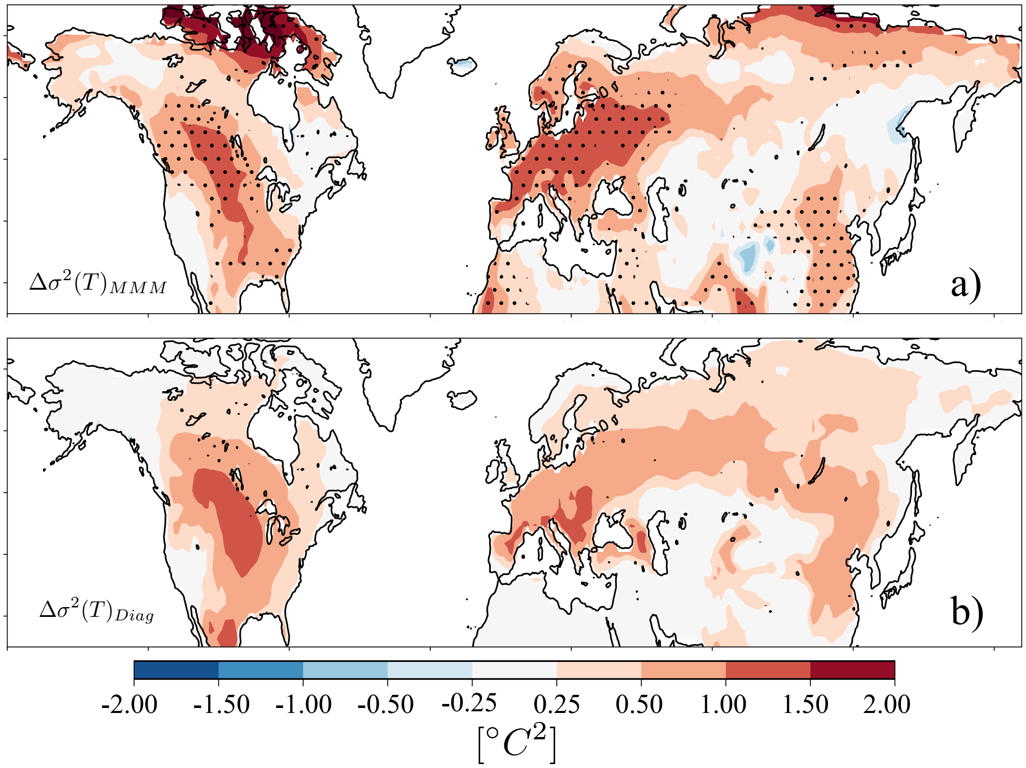

Figure 2. The changes in variance of summertime monthly mean temperatures over the 21$^{\text{st}}$ century (2080-99 of the SSP585 emissions scenario minus 1995-2014 of the historical simulations) in the CMIP6 ensemble mean and (b) predicted from Eq. 5. Stippling in panel (a) shows regions where more than 75% of the models in the ensemble agree on the sign of the variance change.

Fig. 2b shows the pattern of temperature variance change predicted by Eq. 5. The three contributions to temperature variance change on the right-hand-side of Eq. 2 are shown in the supplementary information (Fig. S4). The first two terms contribute most of the change, suggesting that increased aridity with warming acts to amplify the evapotranspiration anomalies in regions with high precipitation variability. The final term is a small residual and does not contribute much to the spatial pattern shown in either panel of Fig. 2.

Given the simplicity of our calculation, the agreement between the two projections is surprisingly good; the increases in summertime temperature variance shown in Fig. 2 represent a 30-50% increase from the historical period (a map of the increases represented as a percentage is shown in Fig. S5). The Central United States, Europe, and East Asia all stand out as regions where the projected impacts of increasing surface temperature variance will be particularly impactful for international food security (Tigchelaar et al., 2018). Further, public health crises driven by extreme heat waves have devastated Europe multiple times since the start of the 20$^{\text{th}}$ century (Schär et al., 2004; Grumm, 2011); our result suggests that these heat waves will grow more severe in a warming world as the mean *and variance* of summertime temperatures increase. The agreement between our simple model and the CMIP6 ensemble suggests that despite the large biases present in the temperature variance in the CMIP6 model simulations of the historical period, the *changes* projected by the climate models are credible and should be accounted for in policy that seeks to make populations and food systems throughout the midlatitudes more resilient to extreme temperature shocks.

The calculation in Eq. 5 reveals the impact of climatological warming on temperature variance and does not include potential changes in shortwave radiation, precipitation, soil moisture, and model parameters. Another method of calculating the expected temperature variance is to subtract one realization of Eq. 1 that uses the forcings and mean state variables taken from the end of the SSP585 scenario from another that uses the forcings and mean state variables taken from the end of the historical period. This calculation, shown in the supplementary information (Fig. S6), displays the same overall pattern of temperature variance change but poorer overall agreement than the calculation based only on local warming shown in Fig. 2b. This suggests that large scale soil moisture drying or changes in underlying model parameters may compensate for the reduction in radiative and precipitation forcing shown in Fig. S3. Overall, our results indicate that local climatological warming is the dominant control on changes in summertime temperature variance.

In our simple model we have assumed the variance in summertime temperature is due to local (one dimensional) forcing. This assumption is supported by previous studies that demonstrate variability in atmospheric temperature advection does not contribute significantly to summertime temperature variability on monthly time scales, except for parts of far western Europe and near the marginal sea ice in the Arctic (e.g. Holmes et al., 2016). In these regions, the projected increase in the climatological land-sea temperature difference should enhance the variance associated with temperature advection. This may explain why the change in temperature variance predicted by our simple model slightly underestimates the increase in temperature variance projected by the CMIP6 models in western Europe and in the coastal regions of the Arctic.

The Importance of Relative Humidity in Temperature Variance Projections

Using only changes in local summertime temperature and relative humidity, our diagnostic model reproduces the projected changes in summertime temperature variance in the CMIP6 models. The multi-model mean change in relative humidity is shown in Fig. 3a; stippling shows grid cells where more than 75% of the models agree on the sign of the change. Changes in North America and Eurasia are particularly large and robust across models, to understand the relative contribution of local relative humidity changes to the increased temperature variance, we can artificially set $\frac{\partial \overline{\mathrm{RH}}}{\partial \overline{T}} = 0$ in Eq. 3 and recalculate $\Delta\sigma^2(T')$.

The dots in Figs. 3b-c show the temperature variance changes predicted by the full version of Eq. 2 (orange) and the artificial prediction where relative humidity changes are excluded from the analysis (blue) as a function of the MMM value of $\Delta\sigma^2(T')$. In both regions, relative humidity changes are equally important as local warming to the projected increase in temperature variance. Both local warming and decreasing relative humidity act to amplify the local atmospheric water vapor demand. In regions where soil moisture is plentiful due to large annually averaged rainfall (like Eurasia and the central United States) increased atmospheric demand for water vapor allows for large evapotranspiration anomalies that amplify the atmospheric forcing variance, and therefore temperature variance.

Relative humidity changes are of first-order importance to the increased summertime temperature variance projected by climate models in the CMIP6 ensemble, but to what extent does local warming control changes in relative humidity over land? Byrne and O'Gorman (2018) have argued that the change in relative humidity over land surfaces is primarily a product of the differential warming over land and ocean. If this were true, the dominant control of model climate sensitivity on the regional warming patterns found across contemporary climate models suggests that model differences in surface warming should account for differences in the change in local relative humidity over land. Figures 4a-b show the changes in local relative humidity as a function of local temperature changes averaged across the two boxed regions in Fig 3a. Nearly half the variance in rel-

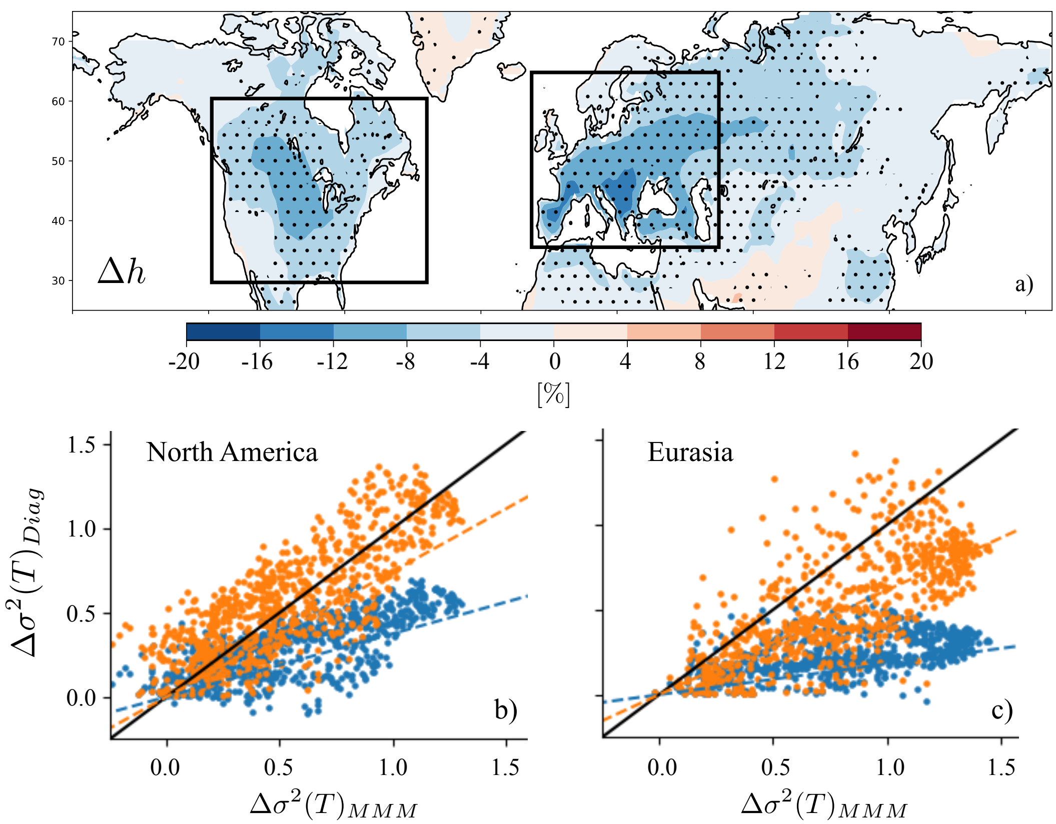

Figure 3. Panel (a) shows CMIP6 multi-model-mean difference in summertime mean relative humidity at the end of the SSP585 experiment and the end of the historical experiment. Stippling shows grid cells where 75% of models agree on the sign of the change. Panels (b) and (c) show comparisons between our simple model's prediction of temperature variance change (y-axis) and the multi-model-mean values (x-axis) in North America and Eurasia, respectively (regions are defined by the black boxes in panel (a)). Orange dots show the calculation when the change in relative humidity is accounted for, blue dots show the calculation when the value of $\frac{\partial \overline{\mathrm{RH}}}{\partial \overline{T}}$ is artificially set to zero.

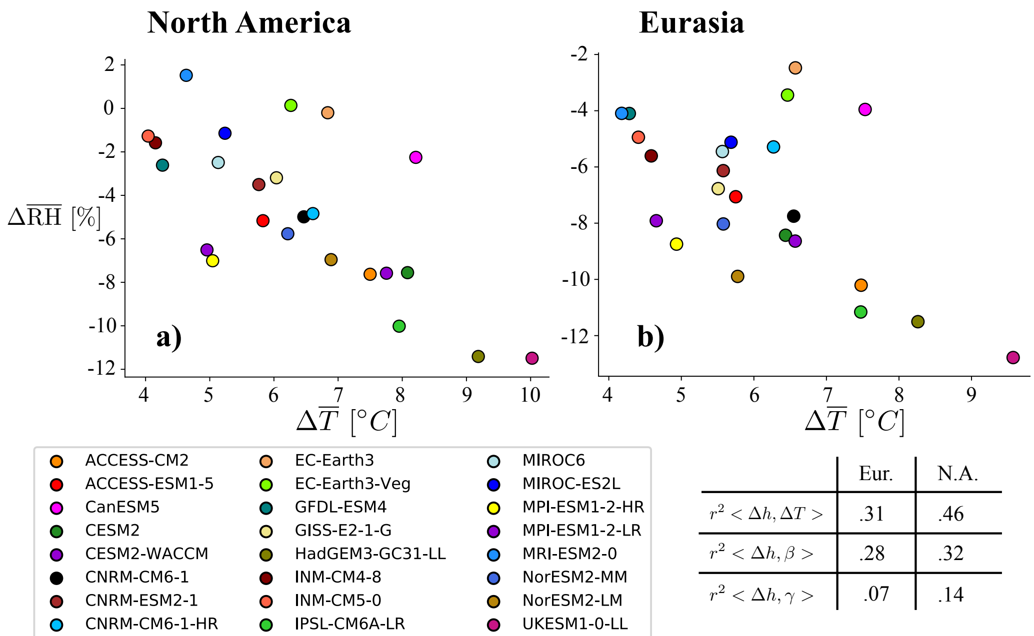

	Eur.	N.A.
$r^2 < \Delta h, \Delta T >$	.31	.46
$r^2 < \Delta h, \beta >$	.28	.32
$r^2 < \Delta h, \gamma >$	.07	.14

Figure 4. Average summertime mean changes in relative humidity across North America (a) and Eurasia (b) between the end of the SSP585 experiment (2080-2099) and the end of the historical period (1995-2014) and as a function of average summertime warming across models participating in the CMIP6 (see legend). The table inset shows the fraction of the inter-model variance in the change in local relative humidity that is explained by local (top) warming, the carbon-concentration feedback parameter (middle) β, and the carbon-climate feedback parameter (bottom) γ from Arora et al. (2019).

ative humidity changes across models (46%) is explained by the local warming over North America, while in Eurasia 31% of the variance is explained by local warming. While local warming is clearly a strong predictor of local changes in relative humidity, other mechanisms are required to explain the inter-model spread within the CMIP6 ensemble.

Plant Activity and Summertime Temperatures

Arora et al. (2019) have calculated sensitivity parameters that quantify the global response of the carbon cycle to increasing CO_2 and temperatures in ten of the models analyzed in Fig. 4. Such parameters necessarily combine numerous plant physiological responses to increasing temperature and atmospheric CO_2 such as increased leaf area, stomatal closure, and a changing growing season start date. The carbon-concentration feedback parameter β quantifies global ecosystem response to a change in atmospheric CO_2: a high β value implies a large increase in land carbon uptake by the land surface in response to increasing CO_2 emissions. One pathway of interest for this study is an increased leaf area driven by a higher atmospheric CO_2 concentration which would increase the mean evapotranspiration in the midlatitudes. The carbon-climate feedback parameter γ quantifies the global ecosystem response to changing mean temperature. The table inset in Fig. 4 shows that of the two parameters, the carbon-concentration feedback value β explains a larger fraction of the inter-model spread of relative humidity change in both Eurasia and North America, comparable to the spread explained by local warming.

Across models, the vegetation response to increasing atmospheric CO_2 is important for the projections of future carbon sequestration and for changes in local relative humidity and, by extension, temperature variance. In models with a large carbon-concentration feedback parameter β, the vegetation response to the increased CO_2 concentration compensates for local warming, likely by increasing leaf area and evapotranspiration thereby reducing the impacts of local warming on relative humidity. Models with a larger leaf area response will therefore exhibit smaller changes in temperature variance due to the mitigating effects on the climatological relative humidity. Differences in the plant response to warming (quantified by the γ parameter values from Arora et al. (2019)) explain more than 10% of the model spread in the climatological relative humidity change in North America; this suggests that modeled plants that are more sensitive to warming mitigate the increase in temperature variance associated with warming by reducing the climatological drying of the atmosphere perhaps by way of earlier leaf-out dates in springtime (Xu et al., 2020).

In general, the spread in the climatological local warming combined with the plant response to climate change explains nearly all of the inter-model differences in the projected change in land summertime relative humidity in North America, where we have already demonstrated that the remote influence of thermal advection on temperature variance is negligible (see Fig. 3b; Holmes et al. (2016)). Over western Eurasia, some of the unexplained variance in relative humidity changes may be due to model differences in temperature advection, but even here we find a large portion of the inter-model spread in the projected change in summertime relative humidity is explained by the combination of local land warming and the plant response to climate change.

Conclusions

A diagnostic model based on monthly equilibrium considerations of the land surface energy and water budgets shows that changes in summertime temperature variance across the midlatitudes are driven in roughly equal parts by local mean warming and decreases in relative humidity. We have shown that despite the high biases in summertime temperature variance present in the CMIP6 models' representation of the historical period (Fig. 1), the model projections of large increases in monthly averaged summertime temperature variance are credible and explained primarily by local warming and its impact on climatological relative humidity.

We have identified two major uncertainties in how summertime temperature variance will change: first, the magnitude of local warming which is primarily controlled by model climate sensitivity. Second, the plant physiological response to CO_2 emissions and how that response changes with mean climate warming. We have shown that models with strong land-carbon cycle responses to increasing atmospheric CO_2 simulate smaller reductions in relative humidity than do models with weak land-carbon responses, indicating that plant activity mitigates the projected reductions in relative humidity that are driven by increasing temperature.

The combination of local warming and plant responses to climate change are the primary contributors to how summertime temperature variability will increase in the future. The diagnostic model and the CMIP6 MMM predict that changes in summertime temperature variance will be greater than $1°C^2$ across much of Eurasia and central North America, representing a 30-50% increase in temperature variance in these regions. Though an assessment of the impacts these kinds of increases in variability would have on the frequency of food shocks and deadly heatwaves is outside the scope of this study, the compounding impacts of a mean warming *and* increasingly temperature variability warrant future study and likely serious policy attention.

Appendix A Methods

This section presents a derivation of Eq. 1, but interested readers can find a more detailed presentation in Vargas Zeppetello et al. (Vargas Zeppetello, Battisti, & Baker, 2020). We begin our derivation by considering the equilibrium land surface energy and water budgets:

$$0 = \mathcal{F}' - F'_{LW} - LE' - H' - G' \tag{A1}$$
$$0 = \mathcal{P}' - E' - R' - I' \ . \tag{A2}$$

All terms in Eq A1 are given in [W m^{-2}], while all terms in Eq. A2 are given in [kg H_2O m^{-2} s^{-1}]. $\mathcal{F}$ is the net downward shortwave radiation incident at the land surface, while F_{LW} is the net upward surface longwave radiation flux. LE and H are the upward turbulent fluxes of latent and sensible heat respectively, while G is the flux of energy downward into the soil column. R and I are the surface runoff and infiltration moisture fluxes respectively, E is the net evapotranspiration, and L is the latent enthalpy of vaporization.

We assume that the sum of monthly net longwave, sensible heat, and ground heat flux anomalies is linearly proportional to temperature fluctuations, thus:

$$F'_{LW} + H' + G' = \nu T' \ . \tag{A3}$$

Here, ν [W m^{-2} K^{-1}] is a parameter that controls the response of two-meter air temperature T' to a radiative forcing $\mathcal{F}'$ in the absence of evapotranspiration anomalies (see Eq. A1).

The sum of runoff and infiltration anomalies is assumed to be linearly proportional to soil moisture fluctuations, thus:

$$R' + I' = \mu m' \ . \tag{A4}$$

The fractional surface saturation m is a unitless number between zero and one that designates the fraction of available pore space in the evapotranspiration-accessible portion of the soil column that is occupied by liquid water. To ensure proper scaling between runoff, infiltration, and precipitation we set the "surface moisture capacity" μ [kg m^{-2} s^{-1}] to be:

$$\mu = \eta \sigma(\mathcal{P}) \ , \tag{A5}$$

where $\sigma(\mathcal{P})$ is the summertime standard deviation in monthly averaged precipitation at each grid cell and η is a unitless parameter that controls the mass of liquid water required to effectively change the soil's fractional saturation m that we assume to be constant everywhere across the land surface.

Total evapotranspiration is given by:

$$E = \frac{\rho_a}{r_s} m V \ . \tag{A6}$$

In Eq. A6, ρ_a [kg air m^{-3}] is the density of air, r_s [s m^{-1}] is the "bulk surface resistance" parameter, V [kg H_2O kg air^{-1}] is a measure of the atmospheric demand for water vapor $q_s(T) - q$ where q_s is the saturation specific humidity at the two-meter air temperature T, and q is the boundary layer specific humidity. We can now define the α parameter used in Eq. 3:

$$\alpha = \frac{r_s \mu}{\rho_a} \ . \tag{A7}$$

The first order terms in a Taylor expansion of Eq. A6 are:

$$E' = \frac{\rho_a}{r_s}[m'\overline{V} + \overline{m}\frac{dq_s}{dT}T'] \ , \tag{A8}$$

where barred terms indicate summertime mean values. In Eq. A8, we have made use of observations and model results that show that anomalies in $\overline{V}$ are overwhelmingly due to anomalies in surface temperature (van Heerwaarden et al., 2010). By substituting Eq. A8 into Eq. A2, we obtain:

$$m' = \frac{1}{\mu + \delta}[\mathcal{P}' - \frac{\rho_a \overline{m}}{r_s}\frac{dq_s}{dT}T'] \ , \tag{A9}$$

where we have defined

$$\delta = \frac{\rho_a \overline{V}}{r_s} \tag{A10}$$

as the climatological mean potential evapotranspiration, or the mean evapotranspiration $\overline{E}$ expected for $\overline{m} = 1$, or saturated soils. Note that δ increases exponentially with $\overline{T}$ according to the Clausius-Clapeyron relationship. Combining Eq. A9 with Eqs. A1 and A8, we obtain:

$$T' = \frac{1}{\Gamma}[\mathcal{F}' - \zeta L \mathcal{P}'] \ , \tag{A11}$$

where $\zeta = (1 + \mu/\delta)^{-1} \subset [0, 1]$ is a dryness index and Γ^{-1} is the "moist surface climate sensitivity":

$$\Gamma = \nu + \frac{L\rho_a \overline{m}}{r_s}\frac{dq_s}{dT}(1 - \zeta) \ . \tag{A12}$$

By squaring Eq. A11 then taking a time average, we arrive at our equation for summertime temperature variance given in Eq. 1:

$$\sigma^2(T) = \frac{1}{\Gamma^2}\left[\sigma^2(\mathcal{F}) - 2\overline{\mathcal{F}'L\mathcal{P}'}\zeta + \sigma^2(L\mathcal{P})\zeta^2\right] \ . \tag{A13}$$

Acknowledgments

This paper contains data from the NOAA ESRL, and the CMIP6 data archive. We are grateful to all who made these data available to the public. The EcoClimate group at the University of Washington provided invaluable feedback during the development of the diagnostic equation and preparation of the manuscript. Marcia Baker helped develop the model and provided feedback on the text of this manuscript. LRVZ was supported by a NSF GRFP Fellowship and DSB was supported by a grant from the Tamaki Foundation. Datasets for this research are available in this in-text data citation reference: (Eyring et al., 2016), with license of CMIP6. Analysis codes and processed data for generating figures in this study are posted at: `https://zenodo.org/record/3877318#.XtqiG55KhTY`.

References

Arora, V. K., Katavouta, A., Williams, R. G., Jones, C. D., Brovkin, V., Friedlingstein, P., ... Ziehn, T. (2019). Carbon-concentration and carbon-climate feedbacks in CMIP6 models, and their comparison to CMIP5 models. *Biogeosciences Discussions*, *2019*, 1–124. doi: 10.5194/bg-2019-473

Berg, A., Lintner, B. R., Findell, K. L., Malyshev, S., Loikith, P. C., & Gentine, P. (2014). Impact of soil moisture - atmosphere interactions on surface temperature distribution. *Journal of Climate*, *27*(21), 7976-7993. doi: 10.1175/JCLI-D-13-00591.1

Berg, A., Sheffield, J., & Milly, P. (2016). Divergent surface and total soil moisture projections under global warming. *Geophysical Research Letters*, *44*(1), 236-244.

Byrne, M. P., & O'Gorman, P. A. (2018). Trends in Continental Temperature and Humidity Directly Linked to Ocean Warming. *Proceedings of the National Academy of Sciences*, *115*(19), 4863–4868. doi: 10.1073/pnas.1722312115

Donat, M. G., Pitman, A. J., & Seneviratne, S. I. (2017). Regional warming of hot extremes accelerated by surface energy fluxes. *Geophysical Research Letters*, *44*(13), 7011-7019. doi: 10.1002/2017GL073733

Eyring, V., Bony, S., Meehl, G. A., Senior, C. A., Stevens, B., Stouffer, R. J., & Taylor, K. E. (2016). Overview of the coupled model intercomparison project phase 6 (cmip6) experimental design and organization. *Geoscientific Model Development*, *9*(5), 1937–1958. doi: 10.5194/gmd-9-1937-2016

Grumm, R. H. (2011). The Central European and Russian Heat Event of July - August 2010. *Bulletin of the American Meteorological Society*, *92*(10), 1285-1296. doi: 10.1175/2011BAMS3174.1

Holmes, C. R., Woollings, T., Hawkins, E., & de Vries, H. (2016). Robust Future Changes in Temperature Variability Under Greenhouse Gas Forcing and the Relationship with Thermal Advection. *Journal of Climate*, *29*(6), 2221-2236. doi: 10.1175/JCLI-D-14-00735.1

Koster, R. D., Suarez, M. J., & Schubert, S. D. (2006). Distinct hydrological signatures in observed historical temperature fields. *Journal of Hydrometeorology*, *7*(5), 1061-1075. doi: 10.1175/JHM530.1

Laguë, M. M., Bonan, G. B., & Swann, A. L. S. (2019). Separating the impact of individual land surface properties on the terrestrial surface energy budget in both the coupled and uncoupled landatmosphere system. *Journal of Climate*, *32*(18), 5725-5744. doi: 10.1175/JCLI-D-18-0812.1

Linz, M., Chen, G., Zhang, B., & Zhang, P. (2020). A framework for understanding how dynamics shape temperature distributions. *Geophysical Research Letters*, *47*(4), e2019GL085684. doi: 10.1029/2019GL085684

Schär, C., Vidale, P., Luthi, D., Frei, C., Häberli, C., Liniger, M., & Appenzeller, C. (2004). The role of increasing temperature variability in European summer heatwaves. *Nature*, *427*(6972), 332-6. doi: 10.1038/nature02300

Schneider, T., Bischoff, T., & Potka, H. (2015). Physics of Changes in Synoptic Midlatitude Temperature Variability. *Journal of Climate*, *28*(6), 2312-2331. doi: 10.1175/JCLI-D-14-00632.1

Seneviratne, S. I., Corti, T., Davin, E. L., Hirschi, M., Jaeger, E. B., Lehner, I., ... Teuling, A. J. (2010). Investigating soil moisture-climate interactions in a changing climate: A review. *Earth Science Reviews*, *99*(3), 125-161.

Tigchelaar, M., Battisti, D. S., Naylor, R. L., & Ray, D. K. (2018). Future Warming Increases Probability of Globally Synchronized Maize Production Shocks. *Proceedings of the National Academy of Sciences*, *115*(26), 6644–6649. doi: 10.1073/pnas.1718031115

van Heerwaarden, C. C., Vil-Guerau de Arellano, J., Gounou, A., Guichard, F., & Couvreux, F. (2010). Understanding the daily cycle of evapotranspiration: A method to quantify the influence of forcings and feedbacks. *Journal of Hydrometeorology*, *11*(6), 1405-1422. doi: 10.1175/2010JHM1272.1

Vargas Zeppetello, L., Battisti, D., & Baker, M. (2020). A new look at the summertime temperature variance over land. *Journal of Climate*, *33*, 5465-5477. doi: 10.1175/JCLI-D-19-0887.1

Vargas Zeppetello, L., Battisti, D. S., & Baker, M. B. (2019). The Origins of Soil Moisture Evaporation 'Regimes'. *Journal of Climate*, *32*(20). doi: 10.1175/JCLI-D-19-0209.1

Vargas Zeppetello, L., Tétreault-Pinard, ., Battisti, D., & Baker, M. (2020). Identifying the sources of continental summertime temperature variance using a diagnostic model of land-atmosphere interactions. *Journal of Climate*, *33*(9), 3547-3564. doi: 10.1175/JCLI-D-19-0276.1

Vogel, M. M., Orth, R., Cheruy, F., Hagemann, S., Lorenz, R., van den Hurk,

B. J. J. M., & Seneviratne, S. I. (2017). Regional amplification of projected changes in extreme temperatures strongly controlled by soil moisture-temperature feedbacks. *Geophysical Research Letters*, *44*(3), 1511-1519. doi: 10.1002/2016GL071235
Willmott, C., & Matsuura, K. (2001). *Terrestrial Air Temperature and Precipitation: Monthly and Annual Time Series (1900-2017) V5.01.* http://climate.geog.udel.edu/climate/html_pages/README.ghcn_ts2.html.
Xu, X., Riley, W., Koven, C., Jia, G., & Zhang, X. (2020). Earlier leaf-out warms air in the north. *Nature Climate Change*, *10*, 370-375. doi: 10.1038/s41558-020-0713-4

Geophysical Research Letters

Supporting Information for

Projected Increases in Summertime Temperature Variance are Driven by Local Thermodynamics

L.R. Vargas Zeppetello, D.S. Battisti

University of Washington Department of Atmospheric Sciences

Contents of this file

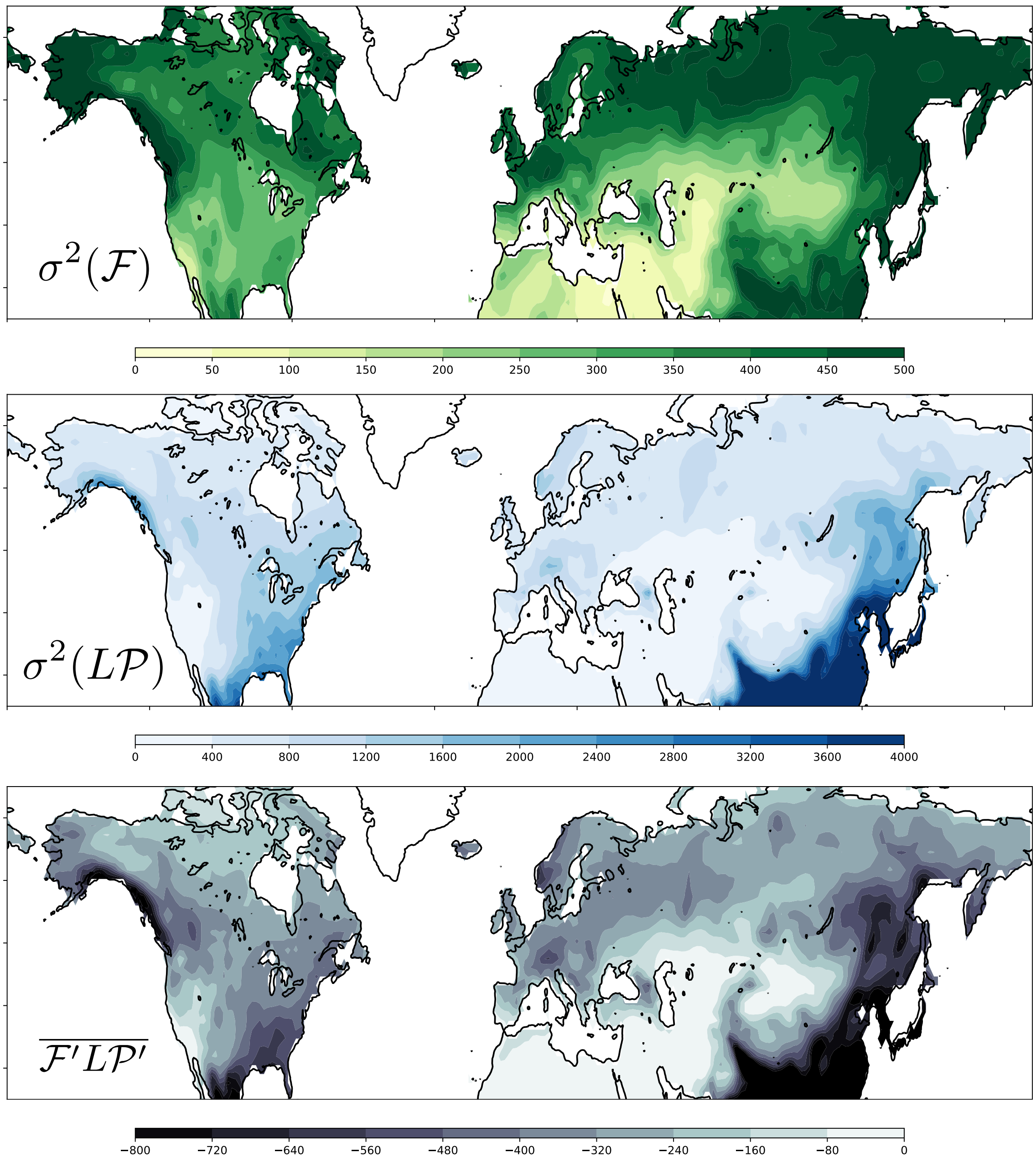

Figure S1: Forcing components used in Eq. 1. All terms given in W^2m^{-4}.

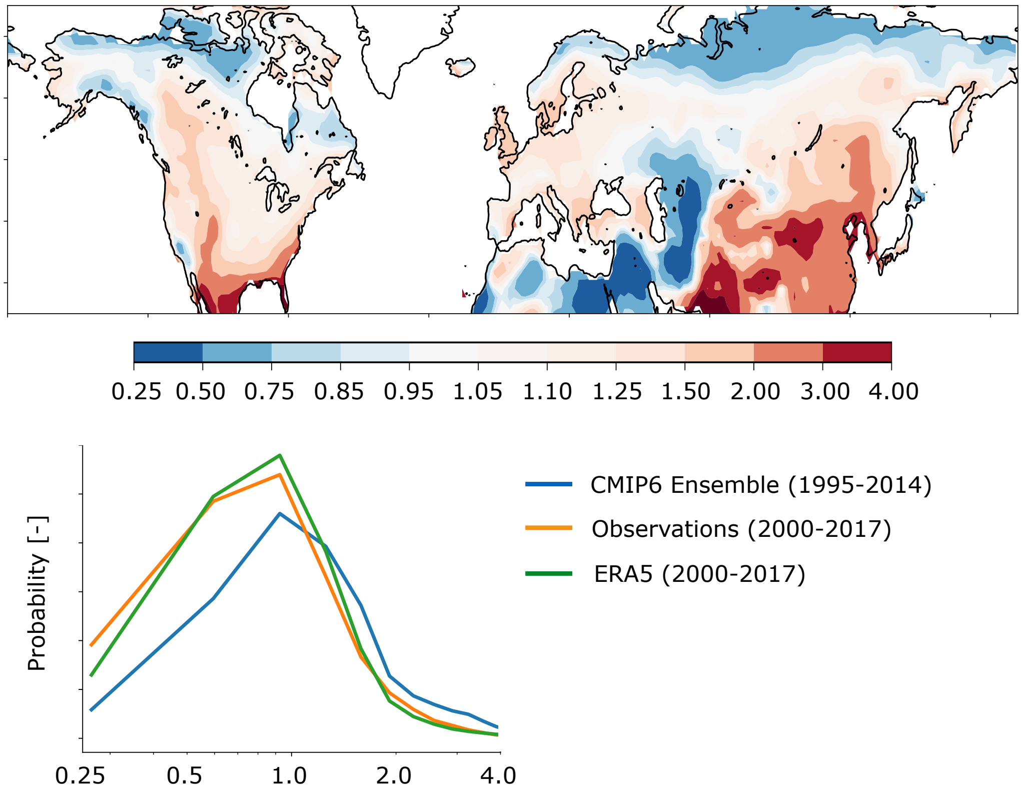

Figure S2: Top panel shows the ratio of temperature variance predicted by Eq. 1 using the forcing components from the CMIP6 ensemble (see Fig. S1) to the temperature variance in the CMIP6 ensemble for the last 20 years of the historical simulations. Bottom panel shows the probability distribution of this variance ratio north of 25˚N for the CMIP6 ensemble (blue), and the variance ratio evaluating the diagnostic equation's accuracy in two other datasets (Observations and ERA5 reanalysis) analyzed in Vargas Zeppetello et al. (in press).

Importantly, while all three realizations of the diagnostic equations use different forcing values and aim to reproduce dataset-specific patterns of temperature variance, all use the same three parameter values for i) dry surface temperature sensitivity (ν), ii) surface resistance (r_s), and iii) soil moisture sensitivity (μ).

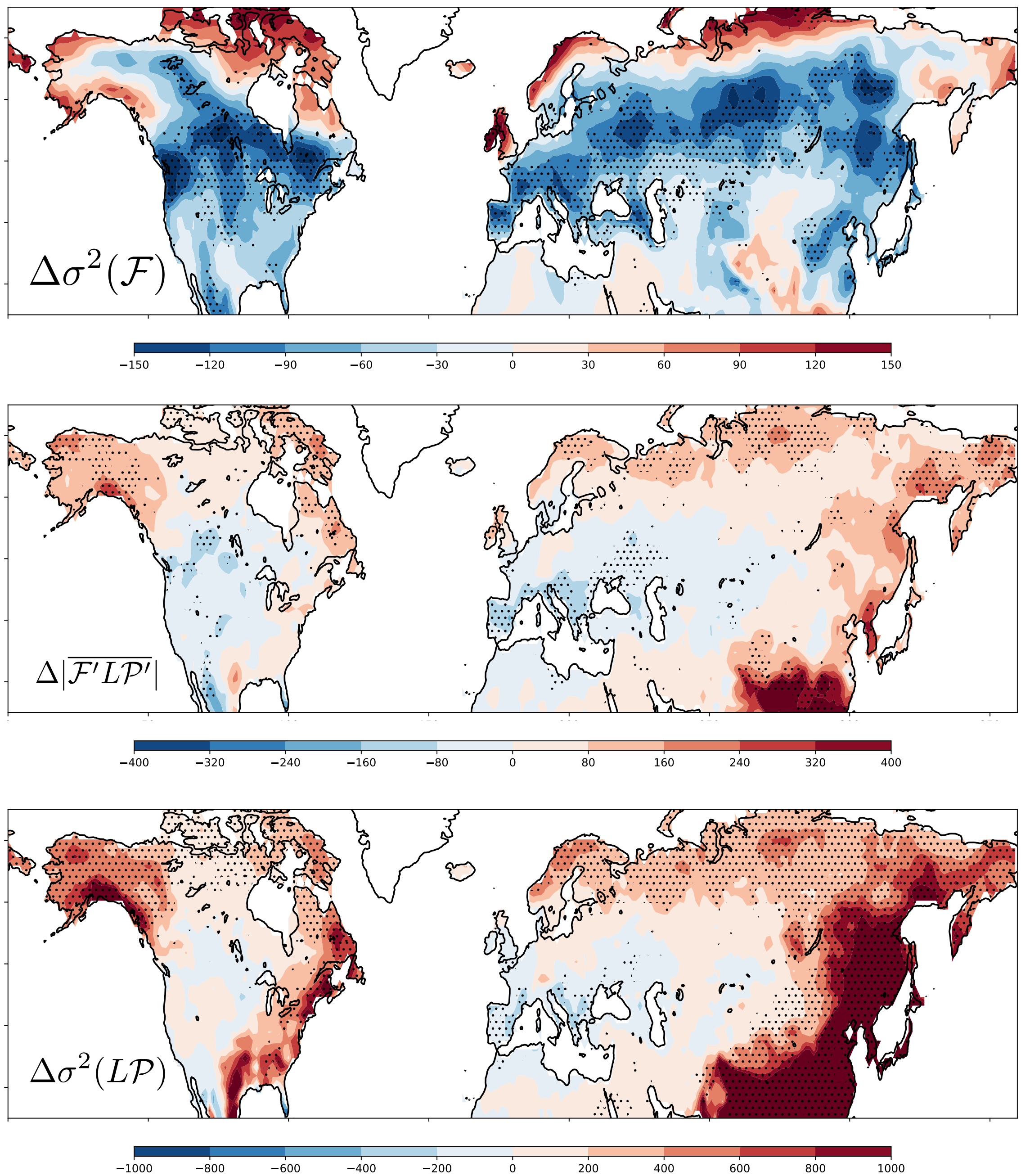

Figure S3: Changes in the forcing components between the end of the SSP585 scenario (2080-2099) and the end of the historical period (1995-2014). All values listed in W^2m^{-4}; dots show the grid cells where more than 75% of the models in the ensemble agree on the sign of the change. Note that the colorbars are different for each plot.

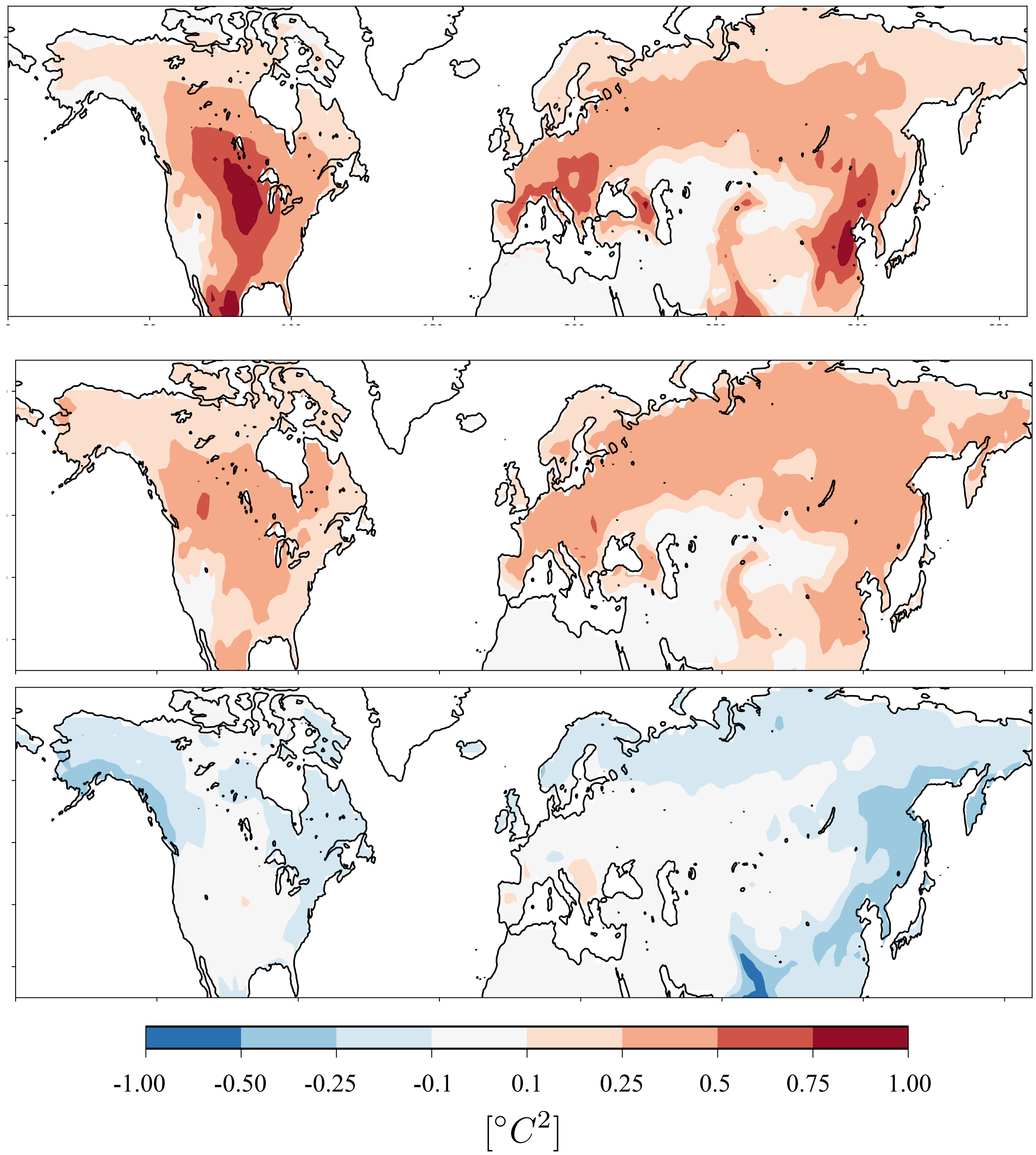

Figure S4: Changes in temperature variance associated with each term in Eq. 2. The top panel shows temperature variance changes associated with amplification of precipitation forcing (first term in Eq. 2), the middle panel shows the changes associated with amplification of the covariance forcing component (second term in Eq. 2), and the bottom panel shows the changes associated with the amplification of the base state temperature variance (third term in Eq. 2).

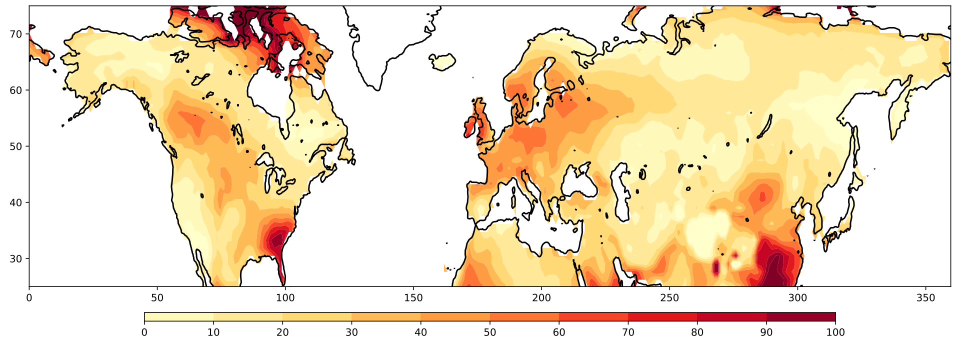

Figure S5: CMIP6 MMM temperature variance change between the end of SSP585 and the end of the historical period shown as a percentage departure from the historical period.

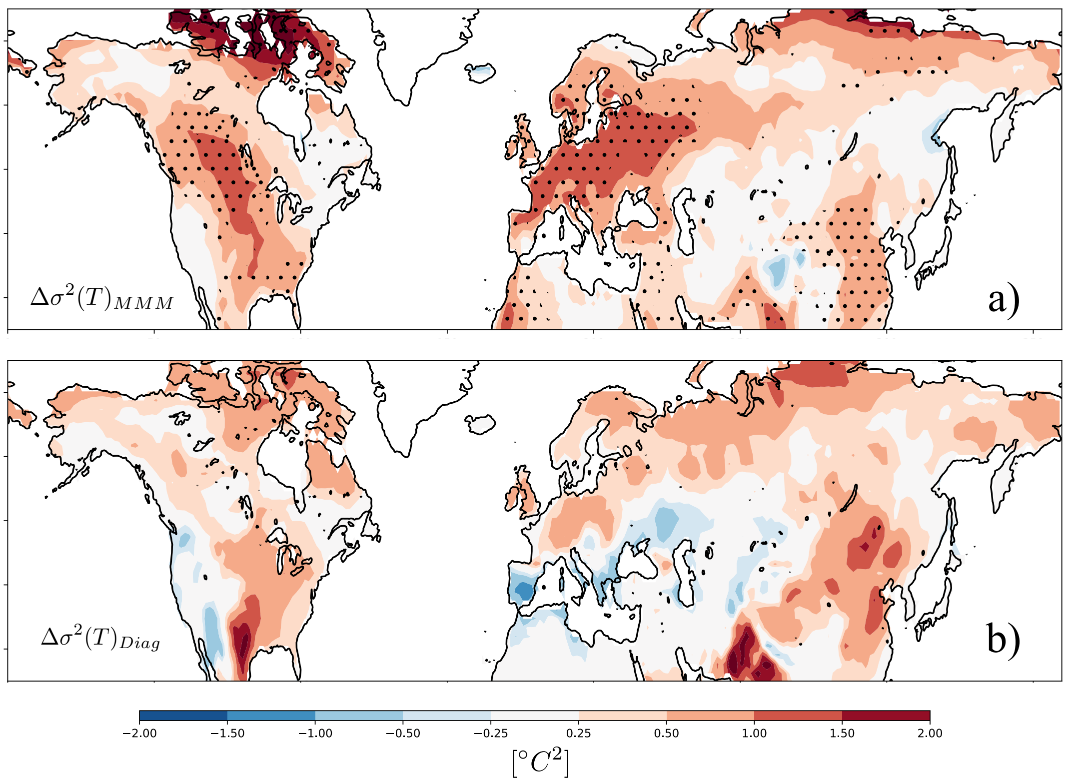

Figure S6: Panel a) is a reproduction of Fig. 2a from the main paper showing the change in temperature variance in the CMIP6 multi-model-mean between the end of the SSP585 scenario and the end of the historical simulations. Panel b) shows the temperature variance change predicted by the diagnostic model taking into account the forcing changes shown in Fig. S3 as well as the summertime warming and relative humidity changes. The agreement is slightly worse than the purely thermodynamic prediction shown in the main paper, for an explanation, see comment above.

Comment on Fig. S6:

The partial derivative taken in Eq. 2 gives the change in temperature variance due only to local warming. Other drivers of temperature variance certainly exist, and additional sensitivity tests of this diagnostic model are shown in Vargas Zeppetello et al. (2020). Figure S6b shows the temperature variance change calculated by subtracting two realizations of Eq. 1 with different values for the forcing components and local summertime mean state variables. We find that the approach presented in the main paper agrees more accurately with the CMIP6 multi-model-mean. This suggests that changes in environmental parameters used in the model or large scale changes in the underlying soil moisture distribution compensate for the changes in the forcing components shown in Fig. S3. These model parameters cannot be estimated from the standard model output and were therefore not considered in our study. However the differences between Figs. S6a, S6b, and 2b indicate that changes in the forcing components, environmental parameters, and underlying soil moisture distribution are of second order importance to the changes associated with local warming outlined in the main paper.

References:

Vargas Zeppetello, L.R., D.S. Battisti, M.B. Baker, 2020. "A New Look at the Variance of Summertime Temperatures Over Land" *J. Climate* 33(13) 5465-5477 doi: 10.1175/JCLI-D-19-0887.1

Model Name	Institution	Model Name	Institution
ACCESS-CM2	Commonwealth Scientific and Industrial Research Organization (Australia)	GISS-E2-1-G-CC	Ibid.
ACCESS-ESM1-5	Ibid.	GISS-E2-1-H	Ibid.
AWI-CM-1-1-MR	Max Planck Institute (Germany)	**HadGEM3-GC31-LL**	Hadley Centre for Climate Prediction and Research (U.K.)
BCC-CSM2-MR	Beijing Climate Center	HadGEM3-GC31-MM	Ibid.
CAMS-CSM1-0	Chinese Academy of Meteorological Sciences	**INM-CM4-8**	Institute for Numerical Mathematics (Russia)
CanESM 5	Environment and Climate Change Canada	**INM-CM5-0**	
CESM2	National Center for Atmospheric Research (U.S.A.)	**IPSL-CM6A-LR**	**Institut Pierre Simon Laplace (France)**
CESM2-WACCM	Ibid.	MCM-UA-1-0	University of Arizona
CNRM-CM6-1	National Centre for Meteorological Research (France)	**MIROC6**	Japan Agency for Marine-Earth Science and Technology
CNRM-CM6-1-HR	Ibid.	**MIROC-ES2L**	Ibid.
CNRM-ESM2-1	Ibid.	MPI-ESM-1-2-HAM	Max Planck Institute (Germany)
E3SM-1-1	Department of Energy (U.S.A.)	**MPI-ESM1-2-HR**	Ibid.
E3SM-1-1-ECA	Ibid.	**MPI-ESM1-2-LR**	Ibid.
EC-Earth3	European Centre for Medium Range Weather Forecast	**MRI-ESM2-0**	International Centre for Theoretical Physics (Italy)
EC-Earth3-Veg	Ibid.	NESM3	Nanjing University of Information Science and Technology
FGOALS-f3-L	Institute of Atmospheric Physics (China)	NorCPM1	Bjerknes Centre for Climate Research (Norway)
FIO-ESM-2-0	First Institute of Oceanography	**NorESM2-LM**	Ibid.
GFDL-CM4	Geophysical Fluid Dynamics Laboratory (U.S.A)	**NorESM2-MM**	Ibid.
GFDL-ESM4	Ibid.	Sam0-UNICON	Seoul National University
GISS-E2-1-G	NASA Goddard Institute for Space Studies (U.S.A.)	**UKESM1-0-LL**	U.K. Met. Office

Table S1: A list of models from the CMIP6 ensemble and their associated modelling institution. All models ran historical simulations, bolded models ran the SSP585 scenario